Dynamics of Bound Monopoles in Artificial Spin Ice: How to Store Energy in Dirac Strings

E. Y. Vedmedenko*
University of Hamburg, Institute for Applied Physics, Jungiusstrasse 11a, 20355 Hamburg, Germany
(Received 17 July 2015; revised manuscript received 27 September 2015; published 17 February 2016)

Dirac strings in spin ices are lines of reversed dipoles joining two quasiparticle excitations. These excitations behave as unbound emergent monopoles if the tension of Dirac strings vanishes. In this Letter, analytical and numerical analysis are used to study the dynamics of two-dimensional dipolar spin ices, artificially created analogs of bulk spin ice, in the regime of bound monopoles. It is shown that, in this regime, strings, rather than monopoles, are effective degrees of freedom explaining the finite-width band of Pauling states. A measurable prediction of path-time dependence of endpoints of a stretched and, then, released Dirac string is made and verified via simulations. It is shown that string dynamics is defined by the characteristic tension-to-mass ratio, which is determined by the fine structure constant and lattice dependent parameter. It is proposed to use string tension to achieve spontaneous magnetic currents. A concept of an energy storing device on the basis of this principle is proposed and illustrated by an experimental demonstration. A scheme of independent measurement at the nanoscale is proposed.

DOI: 10.1103/PhysRevLett.116.077202

Two-dimensional dipolar spin ice (2D-DSI) has been introduced to mimic the three-dimensional dipolar spin ice (3D-DSI) [1] in artificial nanomagnetic arrays [2–4]. 2D-DSI are systems with "macroscopic" degeneracy of ground states in ensembles of magnetic islands with local Ising anisotropy axes coupled by the dipolar interaction and sitting on the square or the kagome lattice. One of the recent developments in spin-ice research concerns the defects also known as "emerging magnetic monopoles" [5–9]. To define the strength of a monopole, each dipole is represented by a dumbbell with charges $\pm q_i$ residing at the vertices of the adjoint lattice, e.g., tetrahedra, squares, or honeycombs. Overturning a dipole leads to emergence of charges $Q_m = \sum_i q_i$. If the tension T_0 of Dirac strings (DSs) connecting two charges of opposite sign vanishes, these charges become unbound [5,10–13]. Unbound monopoles in 3D-DSI are coupled via magnetic Coulomb interaction identical up to a prefactor to that of its electric counterpart [5,10]. While deconfinement in 3D-DSI is easily achieved, one has to go to high temperatures or fields in the case of 2D-DSI [13,14]. Application of a sufficiently strong external magnetic field often results in cascade effects of movement of unbound monopoles. Statistics and criticality of those, field driven avalanches in connected and disconnected square, honeycomb, and kagome networks has been studied in [15–17]. An ongoing discussion concerns the magnetic currents of monopoles in 3D-DSI [1,18] and 2D-DSI [19] defined as "magnetricity". The ultimate goal of this field is the creation of a "magnetic" analogue to electrical circuits [20].

While magnetricity of unbound monopoles has been widely discussed in the literature, the regime of bound monopoles (BMs) remained unexplored until now. A systematic study of confined dynamics, however, is very important because the deconfined regime is vanishing in standard 2D-DSI [6,13,14]. The present investigation shows that, in 2D-DSI, DSs, rather than monopoles, are effective degrees of freedom. Particularly, BMs do not obey the Coulomb law. BMs of opposite sign can be attracted or repulsed depending on the DS tension-to-mass ratio $T_0/2m$, which is defined by the fine-structure constant $\alpha \approx 1/137$ times lattice dependent parameter. It is shown how this peculiarity can be used to achieve spontaneous magnetic currents and to store energy. Spontaneous current in 2D-DSI dies after a certain time. Its duration, however, can be increased by increasing the sample length.

While realistic 2D-DSI may have some degree of disorder on all scales, these calculations are restricted to an ideal ensemble of dipoles for the sake of clarity. The energy of a spin at lattice site i includes contributions from all dipoles on the lattice $E_i = w\sum_j\{[(\mathbf{S}_i \cdot \mathbf{S}_j)/r_{ij}^3] - 3[(\mathbf{S}_i \cdot \mathbf{r}_{ij})(\mathbf{S}_j \cdot \mathbf{r}_{ij})]/r_{ij}^5\}$, where S_i is a unit spin vector. The prefactor $w = (\mu_0\mu^2/4\pi a^3)$, with the magnetic moment μ, magnetic permeability μ_0 and lattice constant a, gives the strength of the interaction. This sum is evaluated numerically using Ewald summation or open boundary conditions. Previous analysis of equilibrium properties of square 2D-DSI has shown that, at experimental temperatures, it should be well in its ordered ground state [6,8]; i.e., the entire sample has to consist of the vertices of type T_1 only (T_1 background in the following, see Fig. 1). The energy of a dipole in an infinite T_1 background is $E_{T1} \approx -5.10$ [w/site]. A saturated square 2D-DSI consists of T_2 vertices only with $E_{T2} \approx -1.51$ [w/site] (T_2 background). The ice state is a statistical

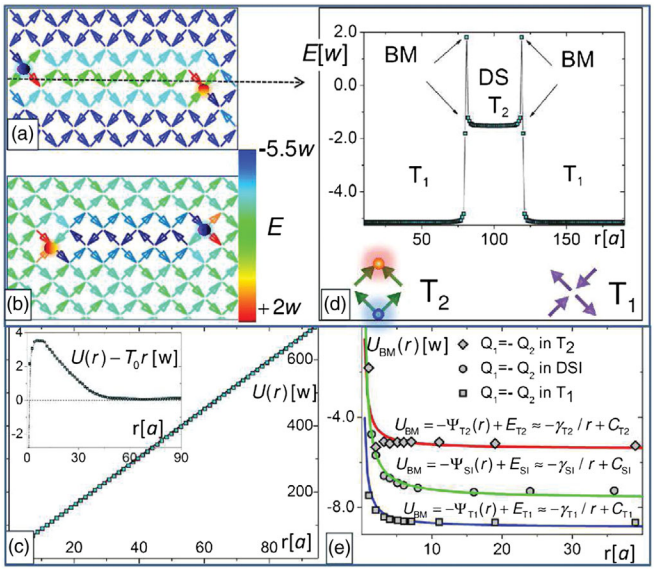

FIG. 1. (a, b) Examples of microscopic configurations used for static calculations. Color scheme gives the energy per dipole. (c) Total energy cost due to formation of DSs of length r in a sample $200a \times 200a$. Numerical data (dots) are fitted by Eq. (1) with $T_0 \approx 7.3w/a$ and $\gamma \approx 0.5wa$. The inset gives the difference between the total potential and the linear term $T_0 r$. (d) Spatial energy profile along the DSs of panel (a) and schematic drawing of T_1 and T_2 vertices. (e) Interaction potential between two BMs of opposite sign in different backgrounds calculated analytically (dots). Lines are fits by function γ/r with $\gamma \approx 1/2$. The γ/r term is repulsive.

mixture of T_1 and T_2 domains [8] defining the band width of Pauling states.

Energy cost of a DS of length r [$U(r) = E_{\mathrm{DS}}(r) - E_{T_1}$] can be fitted by the function $U(r) = -\gamma/r + T_0 r + c$ as postulated in [13,14]. In this expression, T_0 is the DS tension, while γ/r comes from the smeared charge at DS ends [21]. Here, $U(r)$ for strings of Figs. 1(a) and 1(b) has been calculated in samples of different size. Obtained results are in good agreement with those of [14]. However, they show that slope $|dU(r)/dr|$ slightly increases with sample size approaching the value of $T_0 \approx \pm 7.3w/a$ (T_1 and T_2 background, respectively) for $r \gtrsim 70a$ and samples $> 140a \times 140a$ [see Fig. 1(c)]. The critical DS length of $70a$ characterizes the range of the γ/r potential and, hence, the size of charge clouds surrounding BMs. For $r \lesssim 70a$ the BM clouds overlap, for $r > 70a$, but in samples $< 140a$, they are cut off by boundaries.

An important question is whether the limit of $r \approx 70a$ is caused by the numerical accuracy, or if there is a physical reason for this finding. This question is addressed, analytically, in Sec. C of [21]. The main conclusion is that the BM energy cloud is finite. Strictly speaking, γ/r term in $U(r)$ has to be replaced by a similar, but convergent [22], sum of polygamma functions: $\Psi(r) = E_{\mathrm{T1/T2/2D-DSI}} + \sum_{i,n} \psi_n^i(r)$. However, $\Psi(r)$ can be approximated by the standard $1/r$ dependence

$$U(r) \propto T_0 r - \Psi(r) \approx T_0 r - \gamma/r + \mathrm{const}. \quad (1)$$

The localized character of energy peaks around BMs can be seen in the energy profile of Fig. 1(d). The finiteness of BMs permits us to estimate their mass from the mass-energy equivalence $U_{\mathrm{BM}} = mc^2$. The $U_{\mathrm{BM}} \approx U(70a)$, because at $r \approx 70a$ the BM clouds do not overlap, but there is still no free DS between them. As $U(70a) \approx 500w$, the rest mass becomes $m \approx 500w/c^2$. The γ/r term alone is shown in Fig. 1(e). It is weak and always repulsive. The total potential $U(r)$ is attractive ($T_0 > 0$) for a DS in T_1, while repulsive ($T_0 < 0$) for a DS in T_2 background. This conclusion is interesting because it suggests non-Coulomb attraction or repulsion of unlike BMs at any separation. That is, a DS in T_1 will spontaneously shrink, while a DS in T_2 background will spontaneously expand until the regime $T_0 = 0$ is reached. One can use this property for spontaneous magnetricity of BMs without application of an external field.

The dynamics of BMs can be estimated from the second Newton law: $m\ddot{\mathbf{r}} = \mathbf{F}$. The force acting on BMs is $|\mathbf{F}(\mathbf{r})| = -dU(r)/dr \approx \pm T_0 \approx \pm 7.3w/a$ at $r > 70a$ and $|\mathbf{F}(\mathbf{r})| \approx \pm T_0 + \gamma/r^2$ at smaller distances. Solutions of the Newton law in the limit of $\gamma/r \to 0$ and $T_0 r \to 0$ are given by Eq. (2) with L_0 initial DS length (see details in [21])

$$r(t) \approx \begin{cases} L_0 - 2t\sqrt{\frac{L_0 T_0}{2m}} + t^2 \frac{T_0}{2m} & \text{if } \gamma/r \to 0 \\ \left(L_0^{3/2} + 3t\sqrt{\frac{\gamma}{2m}}\right)^{2/3} & \text{if } T_0 r \to 0 \end{cases}. \quad (2)$$

All parameters in Eq. (2) are already known. To check Eq. (2), Monte Carlo (MC) and Landau-Lifshitz-Gilbert spin dynamics (SD) simulations have been performed [21]. Additionally, an experimental model of interacting magnetic elements (see videos SI5–SI6 in [21]) has been built. First, results for atomistic 2D-DSI are presented. Then, calculations for realistic artificial spin ice will be discussed.

Atomistic calculations have been done in the limit of strong coupling; i.e., coercivities of all dipoles were identical and weaker than the intersite interaction. The path-time dependencies of BM motion are shown in Figs. 2(a), 2(b), and in videos SI2–SI4 in [21]. Initially, a DS [Fig. 2(a)] or many such strings [Fig. 2(b)] were created. Next, they were allowed to relax without field. The path-time dependence $r(t)$ of BM movement was recorded and represented in Fig. 2 as density maps. The color and its intensity give the sign and mean strength of BMs. Two scenarios have been checked. In Fig. 2(a), negative BMs (rim dipoles) were pinned, while positive BMs were free to move. In Fig. 2(b), all magnetic moments were free. Once simulations were started, spontaneous BM movement evolved in MC as well as in SD simulations. In contradiction to the Coulomb law, BMs were attracted or repulsed depending on the background (see the videos in the Supplemental Material [21]). Both $r(t)$ dependencies were successfully fitted by Eqs. (2)

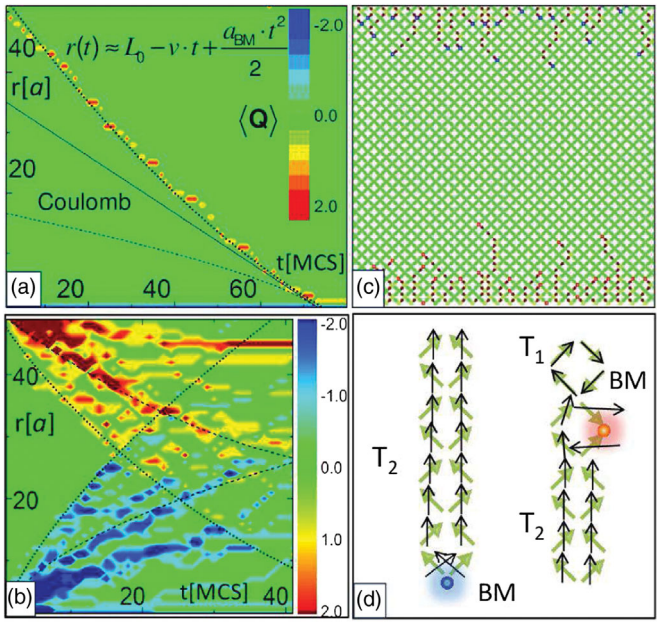

FIG. 2. (a, b) Monte Carlo path-time diagrams of stretched double (a) and multiple DSs (b) at $kT = 0.2w$. The color scheme gives the mean strength of DC at the ends of strings. Initial DS length is $50a$. In (a), a negative BM (blue) is fixed, all other dipoles are free. In (b), all dipoles are free to relax. Numerical data are fitted (lines) by Eq. (2). Dotted line in (a) and dashed line in (b) correspond to $a_{\mathrm{BM}} = T_0/2m \approx 7.3 \times 10^{-3} a/\mathrm{MCS}^2$. In (a), the difference between $r(t)$ of BMs and that of free Coulomb charges is emphasized. In (b), different fronts have different velocities because of local repulsion. (c) gives a snapshot of the path-time diagram in (b) at $t = 5$ MCS. (d) Stray fields (black arrows) in 2D-DSI (green arrows). Stray fields acting on dipoles forming BMs exert torque promoting spin flips.

with $T_0/2m \approx 7.3 \times 10^{-3} \pm 5 \times 10^{-4} a/\mathrm{MCS}^2$. In samples with many DSs, the BMs move in several fronts because of local repulsion [see Fig. 2(b)]. A snapshot at $t = 5$ Monte Carlo steps (MCS) is shown in Fig. 2(c).

The values $T_0 \approx 7.3w/a$ and $2m \approx 10^3 w/c^2$ have already been estimated from the potential $U(r)$ in Fig. 1(c). Please note that numbers 7.3 and 10^3 come from the dimensionless dipolar sum, while dimension is defined by the parameters w/a and w/c^2. Hence, the force between two BMs is proportional to the dimensionless parameter $T_0/2m \approx 7.3 \times 10^{-3}$ times dimensional factor c^2/a. An interesting observation is that $7.3 \times 10^{-3} \approx 1/137$ is close to the fine-structure constant α. To understand this result, one has to recall that in classical electrodynamics the force between the north and south poles of magnetic circuits is $\Phi^2/2\mu_0 A$ with Φ the magnetic flux and A the pole's cross-sectional area. As the flux is carried by Dirac strings, we can use this expression to describe the interaction between BMs. According to the Gauss law the flux from a BM is $\Phi = \oint B dA = \mu_0 Q_m$. On the other hand, the attraction force between two BMs is mainly determined by T_0. Hence, $T_0 \approx \Phi^2/2\mu_0 A = \mu_0 Q_m^2/2A$. The most popular definition of the fine-structure constant is $\alpha = Q_e^2/(4\pi\epsilon_0\hbar c)$ in SI units. In this expression, α is the dimensionless ratio of two constants of proportionality: this of the force ($Q_e^2/4\pi\epsilon_0$) and that of electromagnetic radiation ($\hbar c$). The electron mass is related to $\hbar$ via $m_e = \hbar/c\lambda_C$ with λ_C the Compton length. The fine-structure constant in 2D-DSI is a coefficient in the expression $T_0/2m$. Replacing the m_e by the mass of BMs $m_e \equiv m$, the Compton length by the lattice constant $\lambda_C \equiv a$, and the pole area by $A = 4\pi a^2$, one obtains $T_0/2m \approx (\mu_0/2)(Q_m^2/4\pi\hbar)(c/a) = (\mu_0/2)(Q_m^2/4\pi\hbar c)(c^2/a)$ or $T_0/2m \approx \alpha$ in units of c^2/a. Hence, the appearance of α seems not to be a numerical coincidence but, rather, gives the coupling constant of BM interaction.

To reveal the microscopic reason for the spontaneous BM movement, stray fields $\vec{H}_{\mathrm{st}}$ acting on dipoles in 2D-DSI have been calculated and plotted in Fig. 2(d). Fields (black arrows) acting on dipoles far from BMs are small and do not have any component which is antiparallel to the magnetization $\vec{S}_i$. These fields cannot reverse magnetization. Fields acting on dipoles forming BMs, in contrast, are large ($|H_{\mathrm{st}}| \approx 2\pi\mu_0\mu$), perpendicular, or have a negative component to $\vec{S}_i$. The corresponding torque $\vec{H}_{\mathrm{st}} \times \vec{S}_i$ induces spin flips and, hence, spontaneous movement of BMs decreasing their local energy (any flip transforms T_2 into T_1 vertex). Hence, the microscopic reason for the spontaneous BM drift is local stray fields. Another important observation from the simulations is that the reduction of the string energy $T_0 r$ is achieved by the formation of closed loops consisting of low-energy T_1 vertices only [see Fig. 3(a)]. One infinitely long, ordered closed loop corresponds to the ground T_1 state. The state with many disordered closed loops is nothing but 2D-DSI. The space-time diagram of Fig. 3(a) and video SI3 [21] show that BMs annihilate whenever this leads to formation of a closed loop. The requirement of loop closure can be written mathematically as the Maxwell continuity equation $d\rho/dt + \nabla \cdot \mathbf{j} = 0$, where $\mathbf{j}$ is the current density of monopoles [12,21].

In artificial 2D-DSI, each magnetic element consists of microscopic spins as shown in Figs. 3(b) and 3(c). The energy map of a cross section through the center of elements of a Dirac string in this case is shown in Fig. 3(d). Similar to Fig. 1(d), the T_1 and T_2 regions and BMs are clearly recognizable in Fig. 3(d). The microscopic energy variation corresponds to rims and inner parts of magnetic elements. Mean energy cost $\langle E_{\mathrm{DS}} - E_{T1} \rangle$ per microscopic dipole is different from that of macrospin representation. In the case of 2D-DSI made of $36a \times 24a \times a$ elements, for example, $\langle E_{\mathrm{DS}} - E_{T1} \rangle$/spin is of the order of $0.085w$. Multiplying this value by the number of spins in an element, however, results in $T_0 \approx 7.3w$ for any element size. Hence, the mean string tension in artificial 2D-DSI doesn't change. In artificial 2D-DSI, T_0 has to compete with the shape anisotropy or coercivity E_c. To achieve

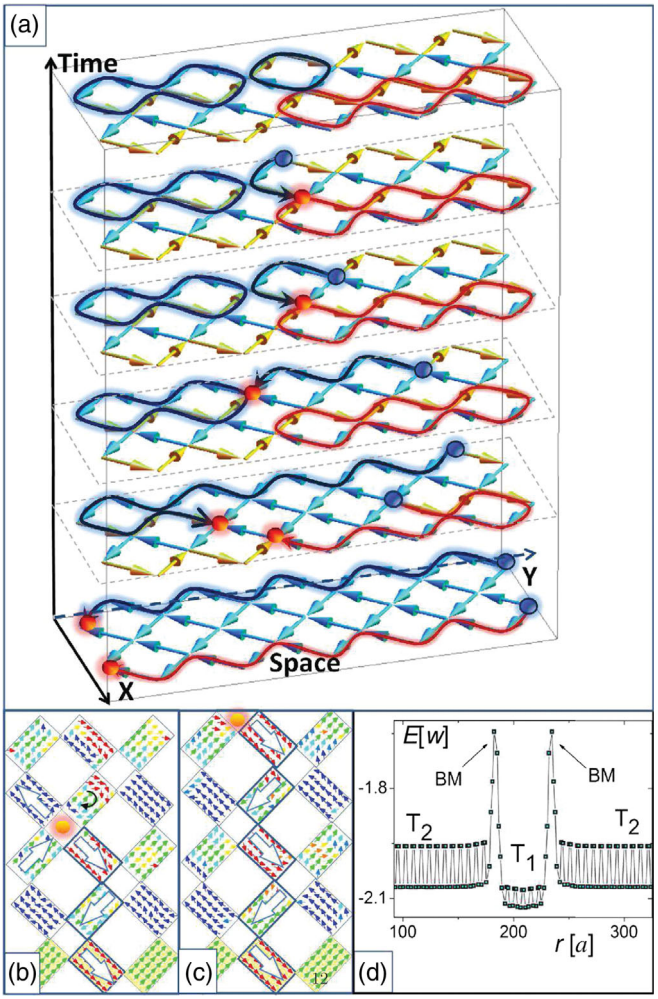

FIG. 3. (a) Space-time diagram constructed from six MC snapshots in $4a \times 10a$ square 2D-DSI with free boundaries. Solid lines and spheres highlight the time evolution of DSs and BMs. (b, c) Two snapshots of a portion of DSs in artificial square 2D-DSI consisting of 10×10 magnetic elements with free boundaries. Each element is made of 24×36 microscopic dipoles. Only each fourth dipole is shown for clarity. Different colors denote different azimuthal orientation of microscopic dipoles. Large arrows give the mean island magnetization. (d) Energy profile in the middle of a static DS in artificial 2D-DSI.

spontaneous dc current, a condition $e^{-[(T_0 r - E_c)/kT]} \gg 0$ has to be satisfied. Hence, the string tension has to be larger than E_c and $k_B T$. In many cases, this condition can be satisfied. An example is given by MC and SD simulations of the 10×10 2D-DSI arrays of Figs. 3(b) and 3(c). The microscopic dipoles $\mu_i = 2\ \mu$B within each element have been coupled by the exchange ($J = 10$ meV) and dipolar interaction. In contrast to studies on connected networks [23], a disconnected 2D-DSI with different element sizes has been checked. The main conclusion is that the spontaneous current can be achieved for elements exceeding sizes $6 \times 9 \times 2$ nm at temperatures $k_B T > 0.25J$. At lower temperatures, the torque due to stray fields is too small to overcome the local coercivities, and an external field has to be additionally applied. Figures 3(b) and 3(c) show two snapshots of a portion of the described array during the BM movement. Magnetization of the three bottom elements was pinned. In contrast to the macrospin picture, the driving stray fields are nonhomogeneous within a magnetic element. The most probable scenario of magnetization reversal is the domain wall formation with its subsequent push out by the stray fields. The magnetization reversal, however, is strongly shape dependent and has to be systematically investigated.

It would be exciting to use spontaneous BMs movement for energy [24] and information storage and to measure $T_0/2m$. The energy can be stored in stretched DSs. The novelty of energy storage in DSs is twofold. First, a string carrying energy of LT_0 can be stabilized by much smaller energy of $2T_0$, because one needs to fix the string ends only, all other dipoles will be pinned by interactions in the local energy minimum as seen in Fig. 1(d). Second, the power $P = dE/dt$ can be tuned geometrically. The $dE = LT_0$ can be stored in one DS of length L or in N parallel strings of length L/N. The dt is determined by the reversal time of one element, which is N times shorter in the second case because of the simultaneous reversal [21]. Hence, long samples provide us with longer currents of weak power, while wide short samples deliver short but powerful currents [21]. The novelty for information storage is the spontaneous character of the BM motion, which is very different from that of domain walls.

To check the above predictions, the following experiments might be performed. Initially, instead of extended arrays, three- or five-row 2D-DSI patches of different length might be studied. The $470 \times 170 \times 3$ nm Py islands with a nearest-neighbor distance of 425 nm [25] would be well suited for photoemission microscopy or x-ray magnetic circular dichroism experiments, while smaller, e.g., $4 \times 2 \times 0.5$ nm, islands from harder magnetic materials for magnetic force microscopy (MFM) measurements. The proposed configuration is benchmarked in the mesoscopic experiment of videos SI5–SI7 [21]. For better controllability, rim islands on one side might have higher coercivity due to, e.g., higher anisotropy, larger magnetization, or local magnetic field. The first act of video SI5 [21] shows that small local fields do not disturb the ground state. If, however, one end is fixed, a small local field from an MFM tip, for example, is enough to form a DS. Alternatively, the DS can be stretched applying global magnetic field. This process is equivalent to the charging of a DS with energy $E = LT_0$. After field removal, the DS might shrink, delivering stored energy (third act of SI5 [21]). The time-resolved imaging of $r(t)$ or time-resolved measurement of stray fields permits determination of tension $T_0/2m$ and current $d\rho/dt$ for given material parameters. Using the dissipative channel of MFM [26,27], the energy needed for this process can be estimated. The

proposed procedure can be repeated for larger 2D-DSI arrays. Video SI6 [21] shows the process of charging and discharging in slow motion.

In conclusion, it is predicted that, maximizing the Dirac string tension, spontaneous magnetic currents can be achieved. On the basis of this prediction, a device for energy storage is proposed and realized in a mesoscopic experimental model. I hope this analysis will encourage experiments and theoretical investigations on confined string dynamics in DSI. These investigations will open broad perspectives relevant to the technology of the future.

This work was supported by the DFG (Grant No. SFB 668). Help by H. Biedermann in creation of the experimental setup and helpful discussions with Professor S. Bramwell, Professor P. Holdsworth, Dr. A. Schwarz, and Professor R. Moessner are gratefully acknowledged.

*Corresponding author.
vedmeden@physnet.uni-hamburg.de

[1] S. T. Bramwell, S. R. Giblin, S. Calder, R. Aldus, D. Prabhakaran, and T. Fennell, Nature (London) **461**, 956 (2009).
[2] R. F. Wang, C. Nisoli, R. S. Freitas, J. Li, W. McConville, B. J. Cooley, N. S. M. S. Lund, C. Leighton, V. H. Crespi, and P. Schiffer, Nature (London) **439**, 303 (2006).
[3] A. Westphalen, A. Schumann, A. Remhof, H. Zabel, M. Karolak, B. Baxevanis, E. Y. Vedmedenko, T. Last, U. Kunze, and T. Eimüller, Phys. Rev. B **77**, 174407 (2008).
[4] N. Rougemaille, F. Montaigne, B. Canals, A. Duluard, D. Lacour, M. Hehn, R. Belkhou, O. Fruchart, S. E. Moussaoui, A. Bendounan *et al.*, Phys. Rev. Lett. **106**, 057209 (2011).
[5] C. Castelnovo, R. Moessner, and S. L. Sondhi, Nature (London) **451**, 42 (2008).
[6] C. Nisoli, R. Moessner, and P. Schiffer, Rev. Mod. Phys. **85**, 1473 (2013).
[7] S. Ladak, D. E. Read, G. K. Perkins, L. F. Cohen, and W. R. Branford, Nat. Phys. **6**, 359 (2010).
[8] J. P. Morgan, A. Stein, S. Langridge, and C. H. Marrows, Nat. Phys. **7**, 75 (2011).
[9] S. J. Blundell, Phys. Rev. Lett. **108**, 147601 (2012).
[10] L. D. C. Jaubert and P. C. W. Holdsworth, J. Phys. Condens. Matter **23**, 164222 (2011).
[11] D. J. P. Morris, D. A. Tennant, S. A. Grigera, B. Klemke, C. Castelnovo, R. Moessner, C. Czternasty, M. Meissner, K. C. Rule, J.-U. Hoffmann *et al.*, Science **326**, 411 (2009).
[12] M. I. Ryzhkin, I. A. Ryzhkin, and S. T. Bramwell, Europhys. Lett. **104**, 37005 (2013).
[13] L. A. S. Mól, W. A. Moura-Melo, and A. R. Pereira, Phys. Rev. B **82**, 054434 (2010).
[14] L. A. S. Mól, R. L. Silva, R. C. Silva, A. R. Pereira, W. A. Moura-Melo, and B. V. Costa, J. Appl. Phys. **106**, 063913 (2009).
[15] H.-B. Braun, Adv. Phys. **61**, 1 (2012).
[16] Y. Shen, O. Petrova, P. Mellado, S. Daunheimer, J. Cumings, and O. Tchernyshyov, New J. Phys. **14**, 035022 (2012).
[17] G. W. Chern, C. Reichhardt, and C. J. O. Reichhardt, New J. Phys. **16**, 063051 (2014).
[18] L. J. Chang, M. R. Lees, G. Balakrishnan, Y.-J. Kao, and D. Hillier, Sci. Rep. **3**, 1881 (2013).
[19] V. Kapaklis, U. B. Arnalds, A. Farhan, R. V. Chopdekar, A. Balan, A. Scholl, L. J. Heyderman, and B. Hjörvarsson, Nat. Nanotechnol. **9**, 514 (2014).
[20] S. R. Giblin, S. T. Bramwell, P. C. W. Holdsworth, D. Prabhakaran, and I. Terry, Nat. Phys. **7**, 252 (2011).
[21] See Supplemental Material SI1–SI6 at http://link.aps.org/supplemental/10.1103/PhysRevLett.116.077202 for description of analytical calculations and video materials.
[22] M. Abramowitz and I. Stegun, *Handbook of Mathematical Functions* (Dover, New York, 1964).
[23] Y. Shen, O. Petrova, P. Mellado, S. Daunheimer, J. Cumings, and O. Tchernyshyov, New J. Phys. **14**, 035022 (2012).
[24] E. Y. Vedmedenko and D. Altwein, Phys. Rev. Lett. **112**, 017206 (2014).
[25] A. Farhan, P. M. Derlet, A. Kleibert, A. Balan, R. V. Chopdekar, M. Wyss, J. Perron, A. Scholl, F. Nolting, and L. J. Heyderman, Phys. Rev. Lett. **111**, 057204 (2013).
[26] P. Grütter, Y. Liu, P. LeBlanc, and U. Dürig, Appl. Phys. Lett. **71**, 279 (1997).
[27] E. Y. Vedmedenko, Q. Zhu, U. Kaiser, A. Schwarz, and R. Wiesendanger, Phys. Rev. B **85**, 174410 (2012).